PRAMANA
— journal of
physics

© Printed in India

Vol. 46, No. 5,
May 1996
pp. 323–329

Time dependent canonical perturbation theory III: Application to a system with nonconstant unperturbed frequencies

MITAXI P MEHTA and B R SITARAM
Physical Research Laboratory, Navrangpura, Ahmedabad 380009, India

MS received 2 November 1995

Abstract. In this communication, we report the results of the application of time dependent perturbation theory to a non-integrable Hamiltonian which is a perturbation on a Hamiltonian with nonconstant frequencies. The theory provides good time dependent local constants of motion and also gives good approximation for mapping of solutions for a time limit determined by the nearest singularity in complex ε plane for fixed real time and the order of calculation.

Keywords. Canonical perturbation; Hamiltonian systems; KAM.

PACS Nos 05·45; 03·20

1. Introduction

Canonical perturbation theory is one of the main mathematical tools to which classical physicists look forward to when a nonlinear Hamiltonian system is encountered. If the given Hamiltonian system has chaotic dynamics, the theory fails in the sense that the generator of the canonical transformation calculated from the theory turns out to be singular [1]. To overcome this problem, use of time-dependent canonical perturbation theory (TCPT) was suggested [2, 3], where time was considered as a new degree of freedom and a canonically conjugate variable T was introduced. It was shown that TCPT removes some of the singularities of the canonical perturbation theory. Our work also suggested existence of natural boundary in complex ε plane for a class of Hamiltonian systems [3]. In this paper we apply the TCPT to the Hamiltonian,

$$H(I_1, I_2, \theta_1, \theta_2) = \frac{I_1^2}{2} + \frac{I_2^2}{2} + \varepsilon(I_1 \cos\theta_2 + I_2 \cos\theta_1). \tag{1}$$

In this paper only the application part is considered, details of TCPT formalism can be found in [2]. The plan of the paper is as follows. Some important aspects of the chosen Hamiltonian system are discussed in § 2. Section 3 discusses the results and conclusion are indicated in § 4.

2. The Hamiltonian

There has been a lot of progress in the analysis of non-integrable Hamiltonian systems which are of KAM [1] type. One important property of these systems is

$$\det\left(\frac{\partial\omega_i}{\partial I_j}\right)\neq 0,$$

where ω_i are unperturbed frequencies and I_j are unperturbed action variables. For comparison of TCPT results with KAM results, we applied TCPT to the Hamiltonian of eq. (1).

This Hamiltonian was chosen because, (1) it is a Hamiltonian on which KAM theory can be applied, (2) the simplicity of the solutions of unperturbed equations of motion makes the application of TCPT simpler. Usually integrable Hamiltonian systems with phase-space dependent frequencies have solutions which are Jacobi-elliptic or related functions of time. TCPT requires integration of H_1 over unperturbed orbits. Integration of the functions of Jacobi-elliptic type is difficult to do analytically whereas for the chosen Hamiltonian system integration of H_1 over unperturbed orbits is easier to calculate.

The Hamiltonian also has scaling property, which can be used to relate the complex-time properties of solutions of equations of motion of H, with complex-ε properties of canonical transformation equations [2], which takes Hamiltonian with $\varepsilon = 1$ to Hamiltonian with some other ε ($\varepsilon \neq 0$). The scaling equations are

$$\theta_i \to \phi_i,$$

$$I_i \to J_i\varepsilon$$

which yields

$$\mathrm{H} = \varepsilon^2 h \tag{2}$$

where

$$h(J_1, J_2, \phi_1, \phi_2) = \frac{J_1^2}{2} + \frac{J_2^2}{2} + (J_1\cos\phi_2 + J_2\cos\phi_1). \tag{3}$$

Thus, as in the case of the Henon–Heiles system [3], studying the system at a fixed energy and different ε values is equivalent to studying the system at a fixed ε value and different energies. Decrease of energy for a fixed value of ε increases the mixing and so gives rise to increase in chaotic behavior. The Hamiltonian has chaotic dynamics at small energy values. As can be seen from the Poincare sections in figures 2a and 2b regular and chaotic dynamics co-exist at the same energy $E = 2{\cdot}0$. In the Poincare sections the variable θ_1 was set to $\pi/2$ on the section and the condition on θ_2 was $\mathrm{mod}(\theta_2, 2\pi) < \pi$ at intersection. The plane of the section is the (I_1, I_2) plane.

3. Results

We used Mathematica programs for calculation of generating functions, invariants and mapping results. All calculations were done with $\varepsilon = 0{\cdot}15$. There are terms in the generator and the invariants with denominators of the form $(n\omega)$ and its powers, which vanish in certain regions of phase-space. The apparent singularities (resonant terms)

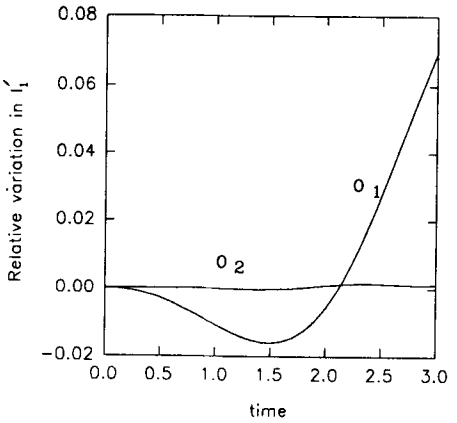

Figure 1a. Relative variation in predicted time-dependent constant of motion I_1' for a regular orbit at $E = 2{\cdot}0$ and $\varepsilon = 0{\cdot}15$. O_1 and O_2 represent first and second order perturbation theory results respectively.

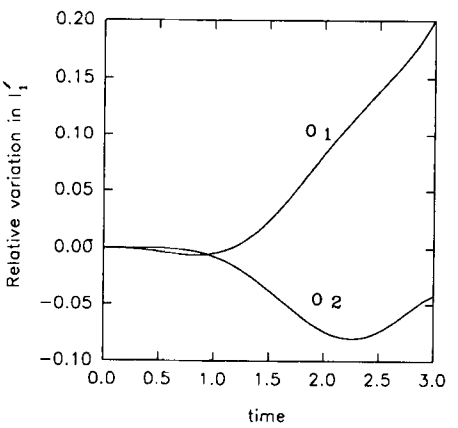

Figure 1b. Same as figure 1a, for a chaotic orbit.

can be removed by taking the limit $(n\omega) \to 0$ in the appropriate regions of phase-space. As expected, the limit turns out to be finite as can be seen from expressions for the first two-order calculation of the generating function and two of their limits are given in appendix A. The limit calculations were also done on Mathematica. The expressions for invariants and mapping of solutions up to nth order are given by the following formulae. Invariants I_i' can be calculated from

$$I_i' = \exp(\varepsilon^n F_n) \cdots \exp(\varepsilon F_1) I_i \tag{4}$$

where I_i represent solutions for equations of motion for H. Mapping from solutions ξ_i' of H_0 to solutions ξ_i of H is given by

$$\xi_i = \exp(-\varepsilon F_1)\exp(-\varepsilon^2 F_2) \cdots \exp(-\varepsilon^n F_n)\xi_i'. \tag{5}$$

Note that the transformation appearing in (5) is inverse of what appearing in (4). But in mapping the action-angle variables appearing in RHS are to be evolved using H_0 equations of motion, whereas in (4) the RHS evolves according to equations of motion for H.

For calculation of invariants a Runge–Kutta fourth order algorithm was used. Figure 1a shows the relative variation in I_1' for a regular orbit at energy $= 2{\cdot}0$ (the relative variation is defined as $2*(I_1'(t) - I_1'(0))/(I_1'(t) + I_1'(0))$). Figure 1b shows the same for a chaotic orbit at the same energy $E = 2{\cdot}0$. First and second order results of perturbation theory are shown in figures which are denoted by O_1 and O_2 respectively. To calculate I_1' at different times, the expression for I_1' is calculated analytically in terms of I_1, I_2, θ_1 and θ_2 using (4) and then in this expression the values of I_1, I_2, θ_1 and θ_2 at different times are put in by solving the equations of motion for H numerically. Figures 2a and 2b are the Poincare sections corresponding to the initial conditions of figures 1a and 1b respectively.

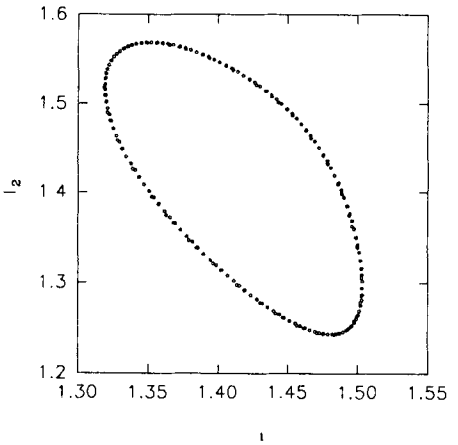

Figure 2a. Poincare section for the regular orbit considered in figure 1a.

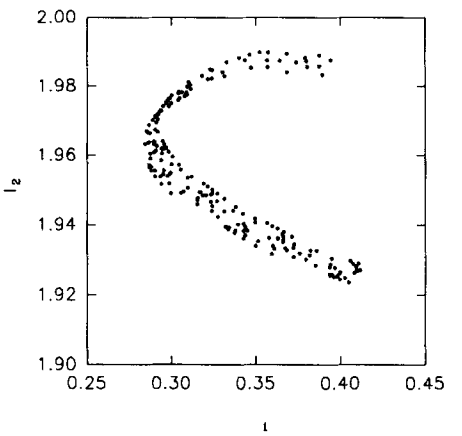

Figure 2b. Poincare section for the chaotic orbit considered in figure 1b.

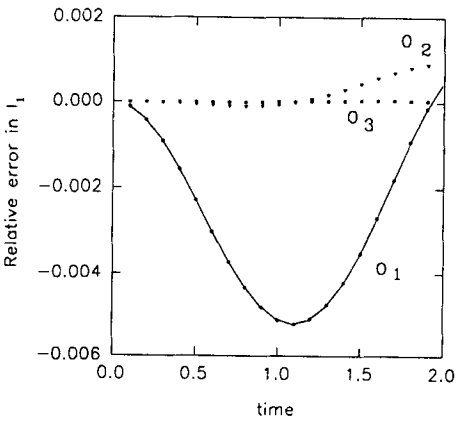

Figure 3a. Relative error in predicted solution for the regular orbit shown in figure 2a. O_1, O_2 and O_3 show first, second and third order calculations repectively. The dotted curves are numerical prediction and the solid curve is the analytical prediction.

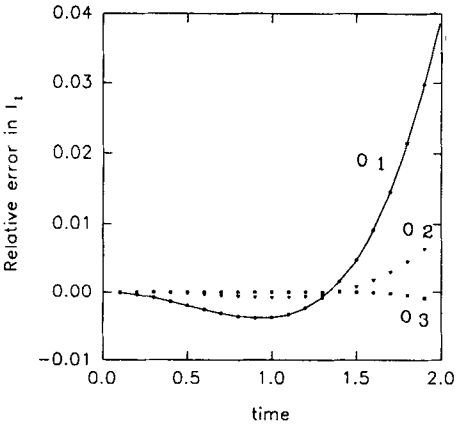

Figure 3b. Same as figure 3a, for the orbit of figure 2b.

Figure 3a shows mapping of solution for regular orbit of figure 2a. The connected line is the relative error in mapped solution with respect to numerically calculated exact solution at first order of calculation. The dotted curves show the relative error at higher orders. (The relative error in mapping is defined as $2(I_{1p}(t) - I_{1n}(t))/(I_{1p}(t) - I_{1n}(t))$ where I_{1p} is the predicted solution and I_{1n} is the numerical solution.) Calculation for mapping at higher orders (shown by dotted curves in the graph) was done numerically using a program that calculates derivatives of the perturbed solution with respect to ε at $\varepsilon = 0$ at given time and initial conditions. The program uses contour-integrals to

calculate derivatives. As figure shows, with higher order calculation in perturbation theory predictions become better. To show that the numerical calculation gives the same result as the analytical one, the first order mapping is calculated using both the methods. Figure 3b is the same as figure 3a, for initial conditions corresponding to the orbit of figure 2b.

We also calculated position of blowing-up singularities (where solutions become infinite) in complex ε plane for real time, which gives the radius of convergence of the perturbation series in ε if there are no other finite singularities (where solutions have finite values). The NAG program d02baf was used with 256 points equally spaced on a circle with centre (0, 0) and radius 0·15 in complex-ε plane, to get evolution of given initial conditions in real time and to find the smallest value of time at which one of the points on the circle has a singular solution. The initial conditions of figure 2a has a singularity at $t \simeq 22{\cdot}6$ and for figure 2b there is a singularity at $t \simeq 11{\cdot}3$.

4. Conclusion

From the analytical and numerical studies of the Hamiltonian system, we can conclude the following:

1. One can use KAM approximation only in the case of irrational tori, whereas our analysis can be used irrespective of the unperturbed frequencies being rational or irrational. It is well-known that KAM predicts total breakdown of perturbation theory even under a very small perturbation but TCPT predicts breakdown of perturbation theory only when a singularity in the complex-ε plane for real time is encountered. It can be easily seen from figures 1a and 1b that TCPT converges for both regular as well as chaotic orbit (broken tori) for small time. At the same time, in TCPT results time appears algebraically and so for convergence at large time, very high order calculations are needed.
2. With the use of TCPT it is possible to establish a relationship between the time dependence and ε dependence of the solutions of a chaotic Hamiltonian for a class of Hamiltonian systems, as shown for the Henon–Heiles system in [2] and for the Hamiltonian studied in this paper.

Appendix A: Generating functions

$$F_1 = \frac{I_2 \sin(\theta_1)}{I_1} + \frac{I_1 \sin(\theta_2)}{I_2} - \frac{I_2 \sin(\theta_1 - I_1 t)}{I_1} - \frac{I_1 \sin(\theta_2 - I_2 t)}{I_2}.$$

$$F_2 = \frac{I_1^2 t}{4I_2^2} + \frac{I_2^2 t}{4I_1^2} + \frac{I_2^2 t \cos(I_1 t)}{4I_1^2} + \frac{I_1^2 t \cos(I_2 t)}{4I_2^2} + \frac{I_2^2 t \cos(2\theta_1 - I_1 t)}{4I_1^2} + \frac{I_1^2 t \cos(2\theta_2 - I_2 t)}{4I_2^2} - \frac{I_2^2 \sin(2\theta_1)}{8I_1^3}$$

$$+\frac{\sin(\theta_1-\theta_2)}{-2I_1+2I_2}+\frac{I_2\sin(\theta_1-\theta_2)}{-4I_1^2+4I_1I_2}$$

$$+\frac{I_1\sin(\theta_1-\theta_2)}{-4I_1I_2+4I_2^2}-\frac{I_1^2\sin(2\theta_2)}{8I_2^3}$$

$$+\frac{\sin(\theta_1+\theta_2)}{2I_1+2I_2}-\frac{I_2\sin(\theta_1+\theta_2)}{4I_1^2+4I_1I_2}$$

$$-\frac{I_1\sin(\theta_1+\theta_2)}{4I_1I_2+4I_2^2}-\frac{I_2^2\sin(I_1t)}{2I_1^3}$$

$$-\frac{I_1^2\sin(I_2t)}{2I_2^3}+\frac{I_2^2\sin(2\theta_1-2I_1t)}{8I_1^3}-\frac{\sin(\theta_1-\theta_2-I_1t)}{4I_1}$$

$$-\frac{\sin(\theta_1-\theta_2-I_1t)}{4I_2}+\frac{\sin(\theta_1+\theta_2-I_1t)}{4I_1}$$

$$-\frac{\sin(\theta_1+\theta_2-I_1t)}{4I_2}+\frac{I_1^2\sin(2\theta_2-2I_2t)}{8I_2^3}-\frac{\sin(\theta_1+\theta_2-I_2t)}{4I_1}$$

$$+\frac{\sin(\theta_1+\theta_2-I_2t)}{4I_2}-\frac{\sin(\theta_1+\theta_2-I_1t-I_2t)}{2I_1+2I_2}$$

$$+\frac{I_2\sin(\theta_1+\theta_2-I_1t-I_2t)}{4I_1^2+4I_1I_2}+\frac{I_1\sin(\theta_1+\theta_2-I_1t-I_2t)}{4I_1I_2+4I_2^2}$$

$$+\frac{\sin(\theta_1-\theta_2+I_2t)}{4I_1}+\frac{\sin(\theta_1-\theta_2+I_2t)}{4I_2}$$

$$-\frac{\sin(\theta_1-\theta_2-I_1t+I_2t)}{-2I_1+2I_2}-\frac{I_2\sin(\theta_1-\theta_2-I_1t+I_2t)}{-4I_1^2+4I_1I_2}$$

$$-\frac{I_1\sin(\theta_1-\theta_2-I_1t+I_2t)}{-4I_1I_2+4I_2^2}.$$

$$\lim_{I_1\to 0}F_1=I_2t\cos(\theta_1).$$

$$\lim_{I_2\to 0}F_1=I_1t\cos(\theta_2).$$

$$\lim_{I_1\to 0}F_2=\frac{\sin(\theta_1)}{12I_2}\times(12\cos(\theta_2)-12\cos(\theta_2-I_2t)-I_2^3t^3\sin(\theta_1)$$

$$+6I_2t\sin(\theta_2)+6I_2t\sin(\theta_2-I_2t)).$$

$$\lim_{I_2\to 0}F_2=\frac{\sin(\theta_2)}{12I_1}\times(12\cos(\theta_1)-12\cos(\theta_1-I_1t)+6I_1t\sin(\theta_1)$$

$$-I_1^3t^3\sin(\theta_2)+6I_1t\sin(\theta_1-I_1t)).$$

References

[1] M V Berry, in *Topics in Nonlinear Dynamics: A tribute to Sir Edward Bullard, AIP Conference Proceedings* edited by S Jorna (AIP, New York, 1978)
[2] B R Sitaram and Mitaxi Mehta, *Pramana – J. Phys.* **45**, 141 (1995)
[3] Mitaxi Mehta and B R Sitaram, *Pramana – J. Phys.* **45**, 149 (1995)